KSME

Springer

Journal of Mechanical Science and Technology 37 (9) 2023

Original Article
DOI 10.1007/s12206-023-0819-5

Keywords:
· Dual-bell nozzle
· Supersonic flow
· Shock wave/boundary layer interaction
· Compressible flow
· Hysteresis

Correspondence to:
Xianghui Su
suxianghui@sina.com

Citation:
Wu, K., Sohn, G. C., Deng, R., Jia, H., Kim, H. D., Su, X. (2023). Study on wall pressure and hysteresis behaviors of a novel dual-bell nozzle. Journal of Mechanical Science and Technology 37 (9) (2023) 4639~4646.
http://doi.org/10.1007/s12206-023-0819-5

Received September 13th, 2022
Revised May 22nd, 2023
Accepted June 5th, 2023

† Recommended by Editor
Han Seo Ko

Study on wall pressure and hysteresis behaviors of a novel dual-bell nozzle

Kexin Wu[1], Gerald Canaan Sohn[1], Ruoyu Deng[2], Hao Jia[1], Heuy Dong Kim[3] and Xianghui Su[1]

[1]Key Laboratory of Fluid Transmission Technology of Zhejiang Province, Zhejiang Sci-Tech University, Hangzhou, China, [2]Department of Control Science and Engineering, Tongji University, Shanghai, China, [3]Department of Mechanical Engineering, Andong National University, Andong, Korea

Abstract The dual-bell nozzle is a kind of altitude adaptive nozzle for improving the performance of space launchers as well as future reusable launch vehicles. Numerical investigations have been conducted on a planar dual-bell nozzle to illustrate the flow characteristics at sea level, “sneak” transition, and altitude modes, respectively. Findings from computational fluid dynamics have been contrasted with experimental data from the open literature. The normalized pressure distributions along the dual-bell nozzle wall for different turbulence models are compared to the pressure measurements taken during the experiment by fixing the nozzle pressure ratio (NPR) at 29.8. The NPR value gradually rises across a large range from 6 to 55 to explore the evolution of the flow characteristics. The pressure distributions along the nozzle wall and shock position have been investigated. The hysteretic behaviors occur in dual-bell nozzles close to the contour inflection. The wall pressure and hysteresis behaviors have been expounded in detail.

1. Introduction

Th All types of rockets that attain high performance primarily depend on the engine's ability to provide more thrust with a simpler structure design and fewer mechanical moving parts [1]. The traditional bell nozzles have been used extensively in recent decades in a variety of contemporary engines for the aerospace industry. The fixed shape of the bell nozzle, however, restricts the engine's comprehensive performance throughout the ascent phase. To meet the performance requirements of the traditional bell nozzle throughout the design phase, some compromises must be made. Some other components that contribute to thrust losses are quite important [2]. Fig. 1 shows various thrust losses in a conventional bell nozzle, which primarily stem from a flaw in the mixing, vaporization, combustion processes, chemical non-equilibrium, recompression shocks, friction, heat loss, interactions with the atmosphere, flow separation in over-expanded situations, divergence, and non-uniformity of exit flow. The engines that use traditional bell nozzles have their comprehensive performance constrained by the aforementioned causes.

Considerable improvements in engine performance can be realized across all operating conditions if the nozzle has the capability of continually adjusting the effective expansion area ratio [3]. Frey et al. [4], Hagemann et al. [5], and Perigo et al. [6] studied several altitude-adapting nozzles, such as the plug nozzle, extendible nozzle, and dual-bell nozzle, in search of maximized advantages. However, many constraints prevent the achievement of the objective, including price, weight, cooling issues, and complicated mechanical moving components [7]. Taylor et al. [8] conducted the experimental comparison of the dual-bell and expansion deflection nozzles utilizing the hot gas, in which the operating conditions are 1000 K and 12 bar in pressure. Although the room for improvement is clear in the optimization of both nozzle types, the expansion deflection nozzle suffers deep aspiration drag resulting in underperforming in low NPR regimes. Hence, it has been excluded as a candidate for main-stage applications and the

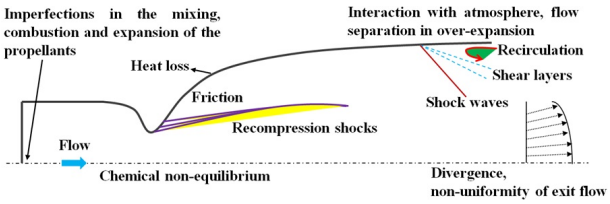

Fig. 1. Flow phenomenon and thrust losses in a conventional bell nozzle.

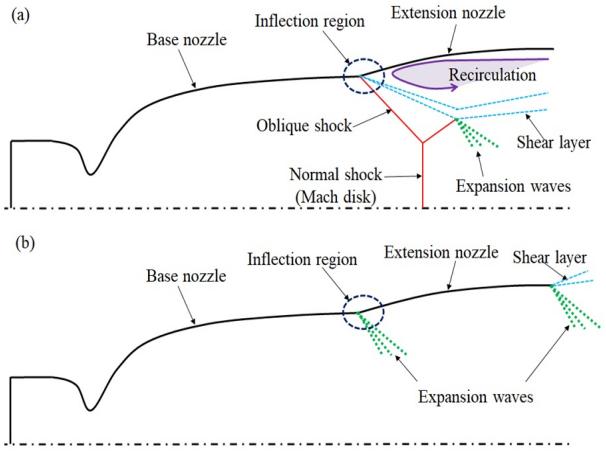

Fig. 2. Phenomenological characteristics in two operation modes: (a) sea-level mode; (b) altitude mode.

adoptions for compact upper stages. The dual-bell nozzle is an attractive design thanks to its relatively simpler design versus plug nozzles, at the compromise of a step-wise altitude compensation instead of a continuous altitude compensation. Even though the dual-bell nozzle makes it possible to reduce the non-adaptation losses in engines working from sea level to almost vacuum conditions, the natural transition between the two modes usually takes place prematurely during the ascent trajectory and destructive side-loads arise. Ferrero et al. [9] demonstrated that fluidic control reduces the order of magnitude of the side load that could arise during the transition process, indicating its potential as an enabling technology for the application of dual-bell nozzles on real engineering applications. Legros et al. [10] expounded on the effects of secondary injection on the dual-bell nozzle, which can allow the transition NPR to be increased by nearly 24 % and the lateral force can be reduced to less than 1 % of the thrust. Stark et al. [11] experimentally found that the operation mode transitions are stable, which are independent of the adjusted cooling film mass flow. Hagemann et al. [12] illustrated the design concept which is relying on the wall contour inflection technique to drive the flow separation at the expected position.

It can be observed in Fig. 2 that the discontinuous wall contour is featured in a dual-bell nozzle which is divided into the upstream part (base nozzle) and downstream part (extension nozzle). Indeed, the wall contour inflection method of single-step altitude adaptation is simply accomplished, and certain design concerns are avoided. To boost engine performance, the effective area ratio must be increased when the flow adheres to the nozzle wall and the dual-bell nozzle exit pressure exceeds the ambient pressure. The symmetrical and regulated flow separations for the sea-level scenarios in Fig. 2(a) are situated near the inflection point. The flow will progressively increase as a result of the ambient pressure lowering and NPR rising as a result. The NPR value reaches a high level, the separation point rapidly moves in the direction of the extension nozzle exit from the inflection point. By definition, the “sneak” transition is a phenomenon wherein, between low-altitude and high-altitude operation modes, there is an intermediate flow condition that occurs before the actual sudden change takes place. In the extension nozzle for the altitude mode in Fig. 2(b), the flow is filled to the top such that the thrust increases continually. On the other hand, Nürnberger-Génin and Stark [13, 14] carried out a series of experiments based on experimental observation to show the phenomenology of the flow by the change from sea-level to high-altitude mode. They demonstrated how the "sneak" transition process is affected by the geometric dimensions of the base and extension nozzles. Davis et al. [15] conducted the numerical and experimental comparison of the flow structure within the proposed dual-bell nozzle contour to those of a conventional nozzle contour and reported that similar flow features are obtained. Génin et al. [16] carried out the experimental and numerical heat flux investigations of the dual-bell nozzle and reported that Ansys Fluent can give an excellent agreement in flow topology and the shape of the shock wave system.

How does hysteresis work? In many natural and artificial systems, when a future event is affected by earlier ones, the hysteresis phenomenon is generally present. In magnetic material fields, it typically exists. Due to several useful engineering applications, research on hysteretic behaviors in compressible flow systems has recently attracted more and more interest. Jiao et al. [17] numerically studied the hysteretic behaviors of the hypersonic inlet at the high Mach number. They argued that the cowl angle and downstream pressure variations can induce hysteresis behaviors. Feng et al. [18] carried out experimental and numerical investigations on hysteresis characteristics in a dual-mode combustor and argued that the wall static pressure distributions of selected feature points depicted an obvious hysteresis phenomenon with the geometry path continuous variation. Chpoun and Ben-Dor [19] conducted numerical simulations to study the shock wave reflection over the straight reflection surfaces in the steady flow and reported the existence of the hysteresis phenomenon from regular reflection to Mach reflection. Later, the shock-reflection hysteresis phenomenon was studied in the low-density and highly under-expanded jet by Gribben et al. [20]. Irie et al. [21] illustrated the hysteresis phenomena, which is caused by the pressure ratio in the under-expanded supersonic dry air jet. Additionally, the distinction between startup and shutdown transients was developed. By manipulating the pressure ratio, Otobe et al. [22] studied the distinctive behavior of the jets during startup and shutdown transient processes and demon-

strated how the hysteresis phenomenon manifests in under-expanded jets. Kim et al. [23] found that the non-equilibrium condensation that took place in the under-expanded settings caused the moist air jets to cause fewer hysteretic behaviors than the dry air jets.

Yasunobu et al. [24] talked about how the shocks of an over-expanded supersonic jet exhibit hysteretic characteristics. Additionally, Matsuo et al. [25] conducted an experimental investigation into the relationship between hysteresis behaviors and the rate of pressure ratio change over time in the context of over-expanded axisymmetric supersonic jets. In addition, Setoguchi et al. [26] investigated the hysteretic behaviors on shock waves in internal flow using experimental and computational approaches, and they showed the connection between the hysteresis behaviors and the rate at which pressure ratios change over time. Wu et al. [27] studied the formation mechanism of the hysteresis phenomenon in a counter-flow thrust vectoring nozzle by changing its pressure ratio. Kumar et al. [28] conducted a numerical analysis to depict the fluid flow and thermal characteristics from a realistic nozzle geometry. Thermodynamically, it is analyzed that compared to medium and low-pressure fluids, the change in fluid density for high-pressure fluids is more substantial hence giving the basics for the hysteresis phenomenon. Verma et al. [29] carried out a two-dimensional axisymmetric simulation to assess the flow characteristics and understand the film cooling process in a dual-bell nozzle. The cooling effect is expounded through the pressure distributions along the dual-bell nozzle wall, in turn, the separation point movement. Nasuti et al. [30] discussed the design of the second bell profile based on results obtained from suitable test cases and found that slightly different geometries designed by the method of characteristics yield modest: performance changes but severe differences in behavior during the transition phase. Barklage et al. [31] analyzed the influence of the Reynolds number on the transition behavior of a dual-bell nozzle with special regard to hysteresis. The comparison of computational and experimental results indicates a consistent shift of the transition to lower values for turbulent flow.

In the present work, the flow characteristics of a particular dual-bell nozzle, with a simple straight extension nozzle contour were studied in detail at a wide range of NPRs. Firstly, the steady work served to illustrate the transition of the shock wave pattern at various stages. The focus was placed in particular on all the defining behaviors that are very close to the "sneak" transition. After that, unsteady simulations were run to indicate the hysteresis phenomenon's presence and impact. Practical implementations of the dual-bell nozzle must be subject to the process of the pressure increasing or decreasing, practically the transition process should be focused especially. Therefore, the current work aims to expound the hysteretic behaviors in the specific transition process by varying the NPR, where the NPR is varied with time linearly. The formation and evolution mechanism of the hysteresis phenomenon in a dual-bell nozzle has been illustrated.

2. Methodology

2.1 Computational model and boundary conditions

The geometry of the dual-bell nozzle with detailed parameters is shown in Fig. 3. A dedicated Table 1 gives the details of the 2D planar nozzle, in which the design chamber conditions, gas properties, and expected performance are demonstrated. Air is a mixture of several gasses in which the two most dominant presences in dry air are 21 % oxygen and 78 % nitrogen, along with 0.934 % argon and carbon dioxide of about 0.03 %. the molecular weight of air is 28.96 g/mol. The dual-bell nozzle consists of two parts, the base nozzle, and the extension nozzle. The base nozzle is selected from a nontruncated ideal nozzle to limit the three-dimensional effects with a Mach number of 2.8. Furthermore, it produces a shock-free flow. For the base nozzle which operates from sea level to high altitudes, the internal shock in the nozzle has a strong influence on the global shock pattern of the exhaust plume and determines the flow separation shock pattern and the side load behavior. If upper-stage engines are not used for stage separation there is no considerable flow separation at the start-up, hence the conical nozzle contour can be used to design the extension nozzle. The numerical simulations are carried out in a 2D planar computational domain, as shown in Fig. 4, and boundary conditions are shown. To achieve an accurate simulation, the computational domain also extends 25 times along the axis and 15 times above and below the dual-bell nozzle exit height. As shown in Fig. 5, a fully structured mesh is created to pre-

Table 1. Details of the 2D dual-bell nozzle.

Parameter	Value
Throat radius (R_{th})	9 mm
Base nozzle area ratio ($\varepsilon_1 = R_1/R_{th}$)	3.9
Extension nozzle area ratio ($\varepsilon_2 = R_2/R_{th}$)	7.1
Base nozzle length (L_1)	135.9 mm
Extension nozzle length (L_2)	107.1 mm
Inflection angle (α)	15°
Total pressure	6-55 bar
Far-field pressure	1 bar
Total temperature	293.15 K
Air (21 % oxygen, 78 % nitrogen, 0.934 % argon, and 0.03 % carbon dioxide)	Ideal gas
Molecular weight	28.96 g/mol
Design Mach number of based nozzle	2.8

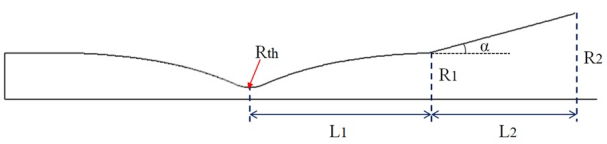

Fig. 3. Geometrical parameters of the planar dual-bell nozzle.

cisely capture the flow phenomenon, and a greater grid density is maintained close to the dual-bell nozzle's throat, inflection point, and exit. After the dual-bell nozzle exits, the gradient grid resolution is retained along the positive axis. For the current geometrical model, the flow field was solved using ANSYS Fluent 18.0. The Reynolds-average Navier-Stokes equation was solved by combining the ideal gas state equation. The density-based server was considered. Implicit formulation and advection upstream splitting method (AUSM) were utilized. More accurate information was reported in the flow field using the second-order upwind scheme. The SST *k-ω* turbulence model is used. By adjusting the inlet total pressure, the dual-bell nozzle properties were steady and unsteady studied for a range of NPRs.

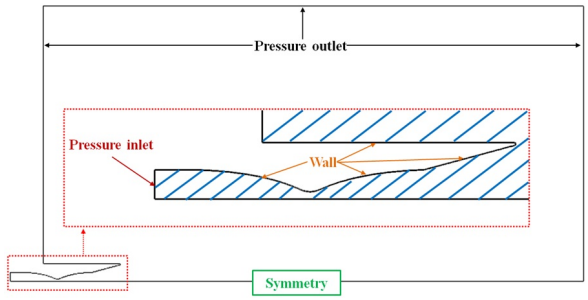

Fig. 4. Computational domain and boundary conditions.

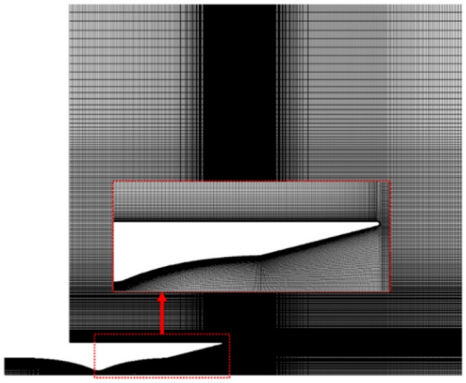

Fig. 5. Partial mesh of the computational domain.

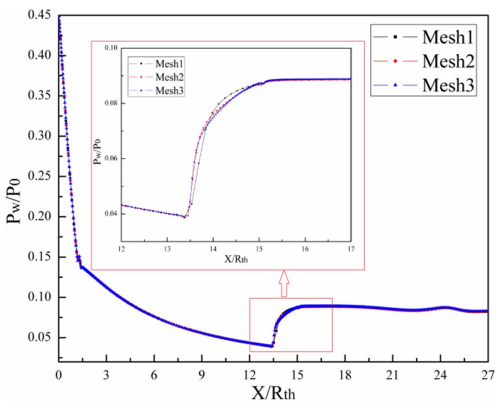

Fig. 6. Static pressure distributions along the nozzle wall for three different grids.

2.2 Mesh independence study

Three resolutions were used for the mesh independence study: 75462 nodes, 158000 nodes, and 291088 nodes. The pressure distributions of several meshes along the dual-bell nozzle wall are shown in Fig. 6 and are used to determine the best resolution for all numerical simulations. It can be observed, there is not much of a difference between grids 2 and 3. The medium grid, which has 158000 nodes, is therefore sufficient for the remaining simulations in the current task.

3. Results and discussion

3.1 Validation

The experiment conducted by Génin et al. [16] was used to validate the current numerical approach. The experimental tests have been carried out within a short test duration between 5 s and 60 s in a steady state. The dual-bell nozzle is mounted on a horizontal test rig and tested for ambient situations at a pressure of 0.1 MPa. The operating conditions of the dual-bell nozzle are that the stagnation pressure is P_0 = 2.98 MPa and the stagnation pressure is T_0 = 293.15 K. Wall pressure measurements were placed along the centerline of the nozzle contour. The numerical simulation was done by using the same boundary conditions as the experiment to validate its accuracy.

The pressure measurements made during the experiment at NPR = 29.8 are contrasted with the normalized pressure distributions throughout the dual-bell nozzle wall for various turbulence models, as shown in Fig. 7. In comparison to the standard *k-ε* turbulence model and the realizable *k-ε* turbulence model, the SST *k-ω* turbulence model shows more accurate agreement with the experimental data recorded by Génin et al. [16]. Therefore, in subsequent numerical simulations, the SST

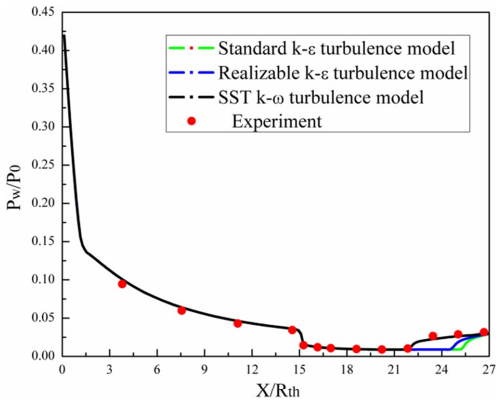

Fig. 7. Comparison of pressure distributions along the dual-bell nozzle wall in CFD result and experiment.

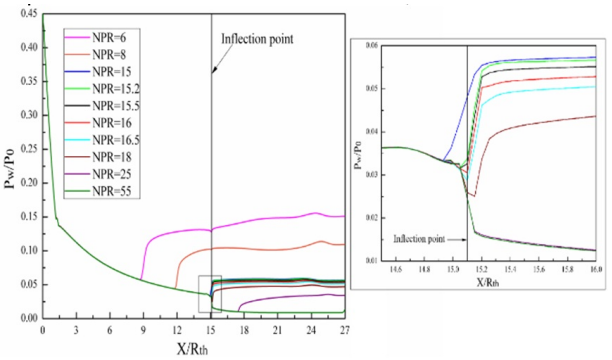

Fig. 8. Pressure distributions along the dual-bell nozzle wall for different NPRs.

k-ω turbulence model is employed to explain the flow behavior of the dual-bell nozzle.

3.2 Effects of NPRs

Fig. 8 illustrates the pressure distributions along the base and extension nozzle wall at various NPRs. The horizontal axis represents the non-dimensional distance and the vertical axis represents the non-dimensional static pressure. The NPR value increases progressively at a wide range (from 6 to 55) to investigate the evolution of flow characteristics and thrust performance respectively. All these cases can be divided into three modes as follows: sea-level mode, sneak transition process, and high-altitude mode. The flow attaches to the base nozzle wall gradually with the increase of NPR (from 6 to 15) while the dual-bell nozzle is in the start-up stage.

Meanwhile, the flow separation moves downstream step by step. Combined with the Mach number contours in Fig. 9, it can be observed that the qualitative variation process on flow characteristics. In addition, some other variations on the shock wave system with the increase of NPR value are depicted in Fig. 9. Normal shock wave (Mach disk) only existed at NPR = 6. It keeps decreasing until it reduces to a point with the increase of NPR value. At NPR = 6, the flow is controlled by the oblique shock wave toward the center line, which is caused by the flow separation. The oblique shock wave hits the normal shock wave at the triple point, and it is reflected as the triple shock wave. Later, the triple shock wave strikes the shear layers and guides the flow parallel to the center line.

The static pressure and streamlines are depicted at NPR = 6 in Fig. 10. The red solid circles make it clear that two areas between the mainline and extension nozzle wall are covered in recirculation bubbles. The static pressure values in these areas are marginally less than the atmospheric pressure value as a result of these recirculation bubbles. Even though it causes an extra thrust loss, the dual-bell nozzle's performance is only marginally impacted. As seen in Figs. 9(b) and (c), the usual shock wave vanished when the NPR value is more than 8. The oblique shock wave impacts the flow, while the shear layers are affected by the reflected shock wave. On the dual-bell nozzle wall, flow separation points were indicated, and it can be seen that the separation point is getting close to the contour inflection point at NPR = 15.

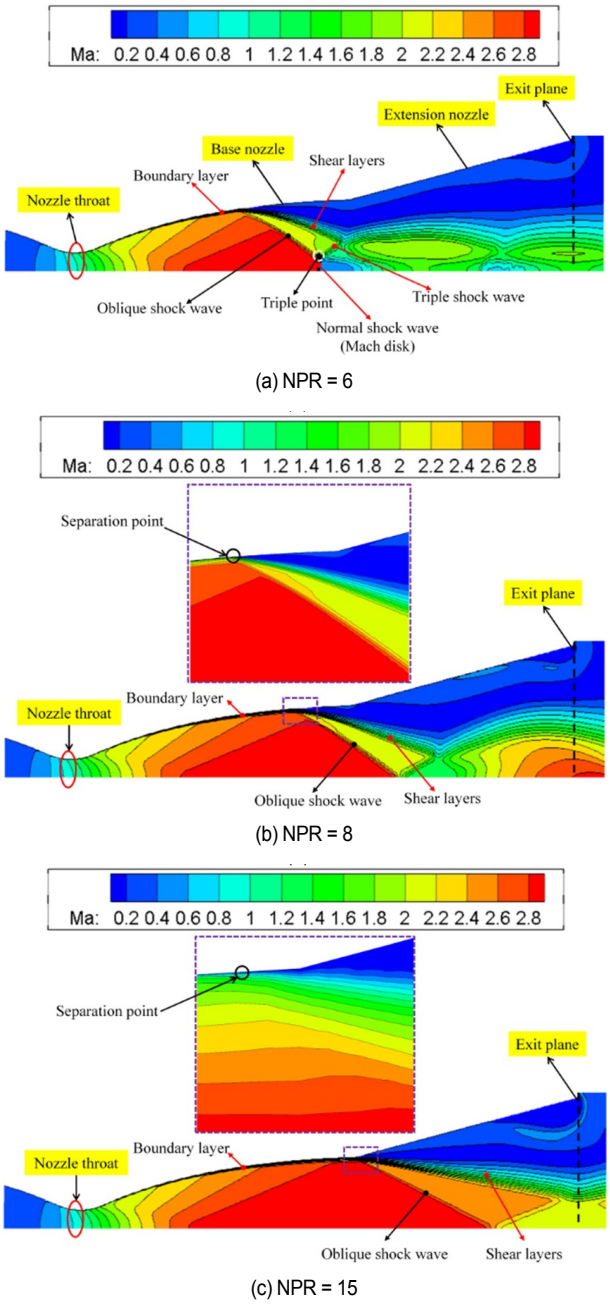

Fig. 9. Sketch of details on the inflection point in the mach number contours at different NPRs.

Additionally, it is evident in Fig. 8 that when the NPR value increases steadily from 15 the separation point position continues to travel downstream along the base nozzle wall. However, when the NPR value fluctuates between 15.2 and 15.5, the separation site is unaffected, due to the formation of pseudo-steady flow separation close to the inflection point. While the flow separation front approaches the inflection point at NPR = 16, it first ceases even if the NPR value keeps rising.

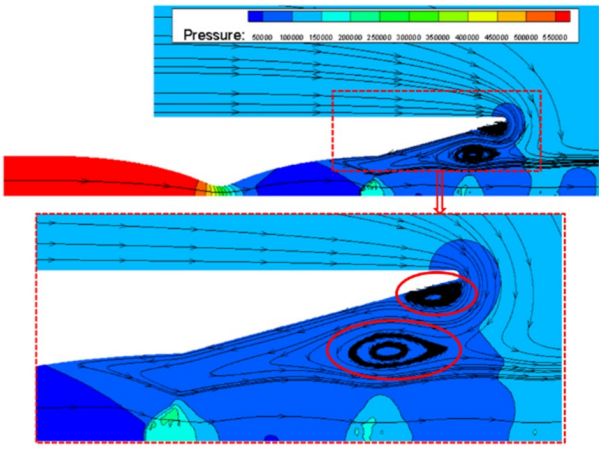

Fig. 10. Details on recirculation flow area in pressure contour at NPR = 6.

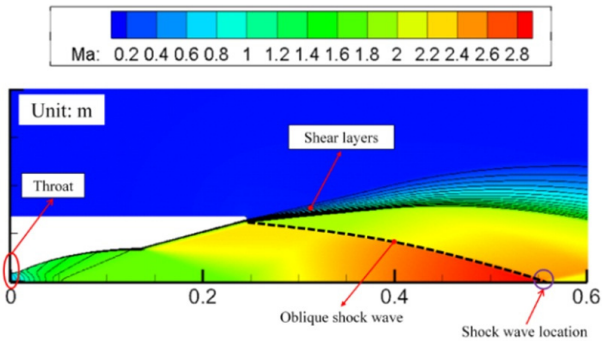

Fig. 11. Mach number contour at NPR = 55.

A constrained range of NPRs stabilizes the flow separation at the contour inflection. The flow separation advances downstream along the extension nozzle where the real changeover will take place when the NPR value continues to rise. The pressure gradient on the dual-bell nozzle wall is negative close to the inflection point, which is defined as the inflection area and has a limited value at the inflection point due to the impact of viscosity. In the remainder of the extension nozzle, the pressure gradient remains constant.

The expectant rapid transition to the altitude mode does not happen and the separation point moves instead progressively down the extension. The altitude option becomes available as the NPR value rises even higher. In particular, the extension nozzle at NPR = 55 has very little pressure dispersion throughout the dual-bell nozzle wall. When seen in conjunction with the Mach number contour in Fig. 11, it is apparent that the flow completely attaches to the extension nozzle, which corresponds to the application of the dual-bell nozzle.

A variety of precise sites for the shock wave, including the previously described normal shock wave and oblique shock wave, are distinguished. Fig. 12 depicts the connection between the NPR value and the precise shock wave position. When the NPR is between 15 and 18, it is seen that the shock wave travels along the nozzle wall slowly as the NPR value rises.

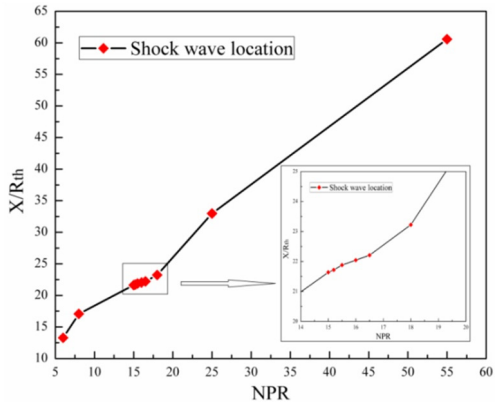

Fig. 12. Shock locations for different NPRs.

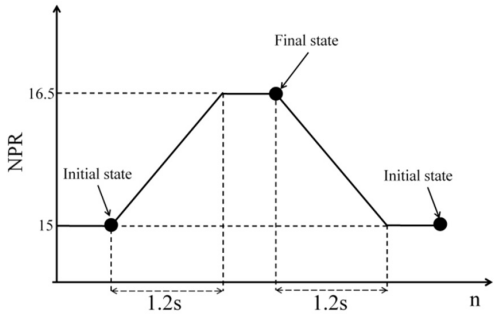

Fig. 13. Computational procedure for varying the NPR value.

3.3 Hysteretic effects of NPRs

Dual-bell nozzles should properly depict the stage where the separation flow is extremely close to the contour inflection for the volatility in NPR value over time due to the formation of side load. The NPR fluctuation process corresponds to hysteresis tendencies in many real situations. As a result, when the NPR value changes linearly from 15 to 16.5, the hysteresis phenomena were investigated. The computational approach used to increase and decrease NPR levels is shown in Fig. 13. The result was used as the beginning condition for the first step of the unsteady case after the steady case calculation. The NPR up-ramping and down-ramping simulations were run. To obtain the final state when it attained the maximum NPR value, an unsteady simulation period was maintained. The NPR value then fell analogously till it reached its starting point. The independent NPR up-ramp or down-ramp started at the same time. The total time for a single increasing or decreasing process was 1.2 seconds and a time step of 10^{-6} was chosen.

Fig. 14 depicts the hysteresis loop on shock movement for various NPRs. The vertical axis displays several non-dimensional shock sites that are derived from the centerline pressure in the up-ramp and down-ramp operations, while the horizontal axis represents the NPR value. Different symbols were used to illustrate the locations of the produced shock waves in the NPR increasing and decreasing processes at the same value. The NPR value corresponds to the computation in

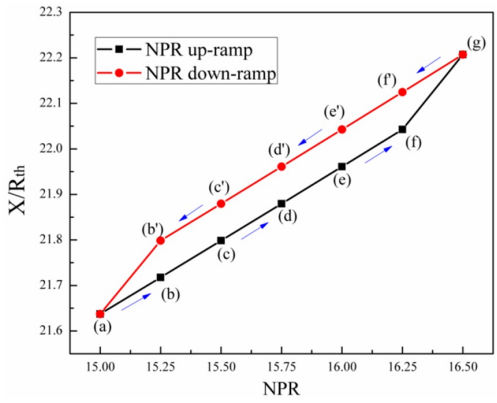

Fig. 14. Hysteresis loop of shock location in NPR up- and down-ramp processes.

Fig. 14 and ranges from 15 (point a) to 16.5 (point g) before returning to 15 (point a). The formation of the hysteresis loop is seen. When the NPR value increases throughout the up-ramp process (from NPR = 15 to NPR = 16.5), the shock wave position shifts downstream. The value of the shock wave location then falls when the NPR value (from NPR = 16.5 to NPR = 15) drops during the NPR down-ramp procedure. Additionally, the obtained shock location values for the NPR down-ramp process are higher than those for the NPR up-ramp process. When compared to the NPR up-ramp procedure, the shock wave travels different paths during the NPR down-ramp stage even if the NPR value is the same. Hence, as per the numerical analysis on the hysteresis loops, the impact of hysteresis on the shock wave is observed. In conclusion, our findings show that the hysteresis phenomenon occurs within the range of changing NPR values and that it had an impact on shock wave migration. The pressure fluctuations caused by the unsteady variations of the recirculation bubbles transmit from downstream to upstream along the subsonic boundary layer affect the hysteresis phenomenon significantly. The large hysteresis effect should be avoided while taking into account the stability of the dual-bell nozzle.

4. Conclusions

As one of the most promising choices for the future, the dual-bell nozzle was demonstrated in achieving high performance. The flow characteristics were studied in a particular dual-bell nozzle within a wide range of NPRs. It was evident that there is an excellent agreement on pressure distributions for NPR = 29.8 between the CFD and experimental results. Pressure distributions along the nozzle wall and shock wave location are discussed.

For sea-level operating mode, the flow is separated symmetrically. The movement of the shock wave is found to be increased rapidly with the increase of NPRs. With the further increase of NPR level, the shock wave moves downstream tardily during the sneak transition process.

The rapid transition to the high-altitude phase does not happen. During the altitude mode, the shock wave starts to move downstream rapidly. The existence of the hysteresis phenomenon was proved when the separation flow is very close to the contour inflection. The change process of the shock wave was well illustrated in changing the NPR with time. The hysteresis loop of shock wave location was formed when the NPR value increases and decreases linearly with time.

Acknowledgments

The authors are grateful for the support from the Natural Science Foundation of Zhejiang Province (Grant No. LQ22E 060002), National Natural Science Foundation of China (Grants No. 52206058, No. 12002241), Zhejiang Sci-Tech University Foundation (Grant No. 21022247-Y), the China Postdoctoral Science Foundation (No. 2020M681393), and Graduate Course Construction Project of Zhejiang Sci-Tech University (Grant No. YKC-202108).

Nomenclature

A	: Exit area
A_t	: Throat area
M_a	: Mach number
$NPRs$	: Nozzle pressure ratios
P_0	: Inlet stagnation pressure
P_a	: Ambient pressure
P_c	: Centreline pressure
P_w	: Static pressure on the nozzle wall
R_1	: Radius of the base nozzle exit
R_2	: Radius of the extension nozzle exit
R_{th}	: Throat radius
T_0	: Stagnation temperature
α	: Inflection angle
ε_1	: Base nozzle area ratio
ε_2	: Extension nozzle area ratio

References

[1] K. Wu, Z. Liu, R. Y. Deng, G. Zhang, Z. C. Zhu, V. R. P. Sethuraman and X. H. Su, Study on the aerodynamic performance of novel bypass shock-induced thrust vector nozzle, *J. Appl. Fluid Mech.*, 16 (4) (2023) 765-777.

[2] H. Kbab, O. Abada and S. Haif, Numerical investigation of supersonic flows on innovative nozzles (dual bell nozzle), *J. Appl. Fluid Mech.*, 16 (4) (2023) 819-829.

[3] J. Östlund, Flow processes in rocket engine nozzles with focus on flow separation and side-loads, *Licentiate Thesis*, Royal Institute of Technology (2022).

[4] M. Frey, A. Preuss, G. Hagemann, S. Girard, T. Alziary De Roquefort, P. Reijasse, R. Stark, K. Hannemann, R. Schwane, D. Perigo, L. Boccaletto and H. Lambare, Joint European effort towards advanced rocket thrust chamber technology, *Proc., 6th Int. Symposium on Launcher Technologies,* Munich, Germany (2005) 1-12.

[5] G. Hagemann, H. Immich, T. V. Nyuyen and G. D. Dumnov, Advanced rocket nozzles, *J. Propul. Power,* 14 (5) (1998) 620-634.
[6] D. Perigo, R. Schwane and H. Wong, A numerical comparison of the flow in conventional and dual bell nozzles in the presence of an unsteady external pressure environment, *Proc. 39th AIAA/ASME/SAE/ASEE Joint Propulsion Conf. and Exhibit,* Huntsville, USA (2003) 1-9.
[7] C. Génin, D. Schneider and R. Stark, Dual-bell nozzle design, *Future Space-Transport-System Components under High Thermal and Mechanical Loads*, Springer, Cham, 146 (2021).
[8] N. Taylor, J. Steelant and R. Bond, Experimental comparison of dual bell and expansion deflection nozzles, *Proc. 47th AIAA/ASME/SAE/ASEE Joint Propulsion Conf. and Exhibit,* Huntsville, USA (2011) 1-13.
[9] A. Ferrero, A. Conte, E. Martelli, F. Nasuti and D. Pastrone, Dual-bell nozzle for space launchers with fluidic control of transition, *Acta Astronaut.*, 193 (2022) 130-137.
[10] B. Legros, L. Léger, A. Kourta, A. Sefir, M. Sellam and A. Chpoun, Fluidic control of flow regime transition and retransition in a dual-bell launcher nozzle, *Proc. Space Propulsion Conf.*, Estoril, Portugal (2022) 1-10.
[11] R. Stark, P. J. Kallina, S. General and D. Schneider, Hot firing of a film-cooled ALM dual-bell nozzle, *Proc. Space Propulsion Conf.*, Estoril, Portugal (2022) 1-10.
[12] G. Hagemann, M. Terhardt, D. Haeseler and M. Frey, Experimental and analytical design verification of the dual bell concept, *J. Propul. Power*, 18 (1) (2002) 116-122.
[13] C. Nürnberger-Génin and R. Stark, Experimental study on flow transition in dual bell nozzles, *J. Propul. Power,* 26 (3) (2010) 497-502.
[14] C. Nürnberger-Génin and R. Stark, Flow transition in dual bell nozzles, *Shock Waves,* 19 (2009) 265-270.
[15] K. Davis, E. Fortner, M. Heard, H. McCallum and H. Putzke, Experimental and computational investigation of a dual-bell nozzle, *Proc., 53rd AIAA Aerospace Sciences Meeting,* Kissimmee, USA (2015) 1-15.
[16] C. Génin, A. Gernoth and R. Stark, Experimental and numerical study of heat flux in dual bell nozzles, *J. Propul. Power,* 29 (1) (2013) 21-26.
[17] X. L. Jiao, J. T. Chang, Z. Q. Wang and D. Yu, Hysteresis phenomenon of hypersonic inlet at high mach number, *Acta Astronaut.,* 128 (2016) 657-668.
[18] S. Feng, J. T. Chang, C. L. Zhang, Y. Y. Wang, J. C. Ma and W. Bao, Experimental and numerical investigation on hysteresis characteristics and formation mechanism for a variable geometry dual-mode combustor, *Aerosp. Sci. Technol.,* 67 (2017) 96-104.
[19] A. Chpoun and G. Ben-Dor, Numerical confirmation of the hysteresis phenomenon in the regular to the Mach reflection transition in steady flows, *Shock Waves*, 5 (4) (1995) 199-203.
[20] B. J. Gribben, K. J. Badcock and B. E. Richards, Numerical study of shock-reflection hysteresis in an underexpanded jet, *AIAA J.*, 38 (2) (2000) 275-283.
[21] T. Irie, H. Kashimura and T. Yasunobu, Hysteresis phenomena of Mach disk formation in an underexpanded jet, *Theor. Appl. Mech.*, 53 (2004) 181-187.
[22] Y. Otobe, T. Yasunobe, H. Kashimura, S. Matsuo, T. Setoguchi and H. D. Kim, Hysteretic phenomenon of underexpanded moist air jet, *AIAA J.*, 47 (12) (2009) 2792-2799.
[23] H. D. Kim, M. S. Kang, Y. Otobe and T. Setoguchi, The effect of non-equilibrium condensation on hysteresis phenomenon of under-expanded jets, *J. Mech. Sci. Technol.,* 23 (3) (2009) 856-867.
[24] T. Yasunobu, K. Matsuoka, H. Kashimura, S. Matsuo and T. Setoguchi, Numerical study for hysteresis phenomena of shock wave reflection in over-expanded axisymmetric supersonic jet, *J. Therm. Sci.,* 15 (3) (2006) 220-225.
[25] S. Matsuo, T. Setoguchi, J. Nagao, M. Md. A. Alam and H. D. Kim, Experimental study on hysteresis phenomena of shock wave structure in an over-expanded axisymmetric jet, *J. Mech. Sci. Technol.*, 25 (2011) 2559-2565.
[26] T. Setoguchi, S. Matsuo, M. M. A. Alam, J. Nagao and H. D. Kim, Hysteresis phenomenon of shock wave in a supersonic nozzle, *J. Therm. Sci.*, 19 (6) (2010) 526-532.
[27] K. X. Wu, Y. Z. Jin and H. D. Kim, Hysteretic behaviors in counter-flow thrust vector control, *J. Aerosp. Eng.*, 32 (4) (2019) 04019041.
[28] M. Kumar, R. K. Sahoo and S. K. Behera, Design and numerical investigation to visualize the fluid flow and thermal characteristics of non-axisymmetric convergent nozzle, *Eng. Sci. Technol. an Int. J.*, 22 (1) (2019) 294-312.
[29] M. Verma, N. Arya and A. De, Investigation of flow characteristics inside a dual bell nozzle with and without film cooling, *Aerosp. Sci. Technol.*, 99 (2020) 105741.
[30] F. Nasuti, E. Martelli and M. Onofri, Role of wall shape on the transition in dual-bell nozzles, *J. Propul. Power*, 21 (2) (2005) 243-250.
[31] A. Barklage, S. Loosen, W. Schröder and R. Radespiel, Reynolds number influence on the hysteresis behavior of a dual-bell nozzle, *Proc. 8th European Conference for Aeronautics and Aerospace Sciences*, Madrid, Spain (2019) 1-11.

Kexin Wu received the Ph.D. degree from Andong National University in the Republic of Korea. Recently, Prof. Wu is working at Zhejiang Sci-Tech University in China. Prof. Wu's research interests involve aeronautics and astronautics, and deep-sea mining.

Heuy-Dong Kim received Ph.D. from Kyushu University in Japan. Recently, Prof. Kim is working at Andong National University in the Republic of Korea. Prof. Kim's research areas involve thrust vector control, pseudo-shock wave, shock wave/boundary layer interactions, shock wave and shock tube, supersonic wind tunnel technology, and high-speed fluid machinery.